

Title	OMARINIITE, $\text{Cu}_8\text{Fe}_2\text{ZnGe}_2\text{S}_{12}$, THE GERMANIUM-ANALOGUE OF STANNOIDITE, A NEW MINERAL SPECIES FROM CAPILLITAS, ARGENTINA
Authors	Bindi, L; Putz, H; Paar, WH; Stanley, CJ
Description	This is a 'preproof' accepted article for Mineralogical Magazine. This version may be subject to change during the production process and you advised to view the published pdf. 10.1180/minmag.2016.080.164
Date Submitted	2017-09-29

OMARINIITE, $\text{Cu}_8\text{Fe}_2\text{ZnGe}_2\text{S}_{12}$, THE GERMANIUM-ANALOGUE OF STANNOIDITE, A NEW MINERAL SPECIES FROM CAPILLITAS, ARGENTINA

LUCA BINDI^{1,*}, HUBERT PUTZ², WERNER H. PAAR³, CHRISTOPHER J. STANLEY⁴

¹*Dipartimento di Scienze de la Terra, Università degli Studi di Firenze, Via G. La Pira, 4, I-50121 Firenze, Italy and CNR – Istituto di Geoscienze e Georisorse, Sezione di Firenze, Via G. La Pira 4, I-50121 Firenze, Italy*

²*Friedl ZT GmbH Rohstoff- und Umwelt Consulting, Karl-Lötsch-Strasse 10, A-4840 Vöcklabruck, Austria*

³*Pezoltgasse 46, A-5020 Salzburg, Austria*

⁴*Natural History Museum, Cromwell Road, London SW7 5BD, United Kingdom*

*Corresponding Author: luca.bindi@unifi.it

ABSTRACT

Omariniite, ideally $\text{Cu}_8\text{Fe}_2\text{ZnGe}_2\text{S}_{12}$, represents the Ge-analogue of stannoidite and was found in bornite-chalcocite-rich ores near the La Rosario vein of the Capillitas epithermal deposit, Catamarca Province, Argentina. The mineral is closely associated with three other Ge-bearing minerals (putzite, catamarcaite, rarely zincobriartite) and bornite, chalcocite, digenite, covellite, sphalerite, tennantite, luzonite, wittichenite, thalcosite and traces of mawsonite. The width of the seams rarely exceeds 60 μm , their length can attain several 100 μm 's. The mineral is opaque, orange-brown in polished section, has a metallic luster and a brownish-black streak. It is brittle, and the fracture is irregular to subconchoidal. Neither cleavage nor parting are observable in the sections. In plane-polarized light omariniite is brownish-orange and has a weak pleochroism. Internal reflections are absent. The mineral is distinctly anisotropic with rotation tints varying between brownish-orange

and greenish-brown. The average result of 45 electron-microprobe analyses is Cu 42.18(34), Fe 9.37(26), Zn 5.17(43), In 0.20(6), Ge 11.62(22), S 31.80(20), total 100.34(46) wt%. The empirical formula, based on $\Sigma(\text{Me}+\text{S}) = 25$, is $\text{Cu}_{8.04}(\text{Fe}_{2.03}\text{In}_{0.02})_{\Sigma 2.05}\text{Zn}_{0.96}\text{Ge}_{1.94}\text{S}_{12.01}$, ideally $\text{Cu}^+_8\text{Fe}^{3+}_2\text{Zn}^{2+}\text{Ge}^{4+}_2\text{S}^{2-}_{12}$. Omariniite is orthorhombic, space group $I222$, with unit-cell parameters: $a = 10.774(1)$, $b = 5.3921(5)$, $c = 16.085(2)$ Å, $V = 934.5(2)$ Å³, $a:b:c = 1.9981:1:2.9831$, $Z = 2$. X-ray single-crystal studies ($R_1 = 0.023$) revealed the structure to be a sphalerite derivative identical to that of stannoidite. Omariniite is named after Dr. Ricardo Héctor Omarini (1946–2015), Professor at the University of Salta, for his numerous contributions to the geology of Argentina.

Keywords: omariniite, new mineral species, copper-iron-zinc-germanium-sulfide, electron-microprobe analyses, reflectance data, crystal structure, La Rosario vein, Capillitas district, Catamarca Province, Argentina.

INTRODUCTION

Omariniite is one of the six germanium-bearing sulfides occurring at Capillitas; among them, putzite, $(\text{Cu}_{4.7}\text{Ag}_{3.3})_{\Sigma 8}\text{GeS}_6$ (Paar *et al.*, 2004), catamarcaite, Cu_6GeWS_8 (Putz *et al.*, 2006), and omariniite, previously named “Ge-stannoidite” (Paar *et al.*, 2004; Putz, 2005; Putz *et al.*, 2006), have here their type-locality. Other two species, spryite (Bindi *et al.*, 2016) and zincobriartite (McDonald *et al.*, 2016) were first recognized at Capillitas and described as Zn-dominant briartite and “As-argyrodite” (Putz *et al.*, 2002; Putz, 2005). The full characterization and description as new mineral species were later given by McDonald *et al.* (2016) and Bindi *et al.* (2016) who described zincobriartite and spryite, respectively. In addition, the Capillitas epithermal deposit is the type locality for the

minerals ishiharaite, ideally $(\text{Cu,Ga,Fe,In,Zn})\text{S}$ (Márquez-Zavalía *et al.*, 2015), and
liskirchnerite, ideally $\text{Pb}_6\text{Al}(\text{OH})_8\text{Cl}_2(\text{NO}_3)_5 \cdot 2\text{H}_2\text{O}$ (IMA No. 2015-064, Effenberger *et al.*,
2015).

Two further germanium-bearing sulfides - germanite and renierite - are said to occur
at Capillitas. They were first reported by Márquez-Zavalía (1988) on the basis of ore
microscopic investigations, but have never been analyzed by electron microprobe or X-ray
techniques. Most probably, they have been misidentified with nekrasovite (“germanite”)
and vinciennite (“renierite”). Both nekrasovite and vinciennite have been frequently
observed in high-sulfidation stage ore from several veins of the Capillitas deposit (Putz
2005). Thus, the occurrence of germanite and renierite remains uncertain.

According to Höll *et al.* (2007) Cu-Fe-Zn-Ge-sulfides like germanite and renierite are
characteristic for the carbonate-hosted Kipushi-type polymetallic deposits (e.g. Tsumeb,
Namibia, and Kipushi, Democratic Republic of Congo) but also occur within high-
sulfidation epithermal Cu-Au deposits (e.g. Chelopech, Bulgaria). On the contrary,
argyrodite is typically observed in bonanza-grade silver mineralization of the Bolivian “Ag-
Sn-belt” (e.g. Porco and Colquechaca Ag-Zn-Pb-Sn deposits, Bolivia; Paar and Putz,
2005) and in vein-type Ag-Pb-Zn(-Cu) deposits (e.g. Freiberg district, Saxony, Germany;
Höll *et al.*, 2007). The mineralogy and distribution of germanium at Capillitas is thus unique
on a worldwide scale and represents a new mode of the occurrence of this rare metal in
epithermal systems. In addition to the six mentioned germanium minerals, Ge contents up
to 0.2 wt.% have been found in colusite-nekrasovite (Putz, 2005). This germanium
anomaly was discovered during the PhD project of one of the authors (HP), which included
a detailed study of the complex mineralogy at Capillitas.

Omariniite is named in honor of Dr. Ricardo Héctor Omarini (1946–2015), Professor at the University of Salta, for his outstanding contributions to the geology of Argentina, especially to the Precambrian basement of the “Formación Puncoviscana”.

The mineral and the mineral name have been approved by the IMA CNMNC (2016-050). Holotype material is housed within the Systematic Reference Series of the National Mineral Collection of Canada, Geological Survey of Canada, Ottawa, Ontario, under catalogue number NMCC 68096. Cotype material is deposited within the collections of the University of Firenze (Italy), the Natural History Museum of London (UK) and in the private collections of two of the authors (HP and WHP).

LOCATION, GEOLOGY AND MINERALIZATION

The Capillitas mining district is part of the Farallón Negro Volcanic Complex (FNVC), which is located in the Province of Catamarca, Argentina. It consists of Miocene extrusive and intrusive subvolcanic rocks within the crystalline basement (metapelites and schists of the Suncho Formation and Capillitas granitic batholith). Porphyry copper-gold deposits (e.g. Bajo de La Alumbreira, Agua Rica) and epithermal vein-type deposits (e.g. Capillitas, Farallón Negro - Alto de la Blenda) are associated with the intrusive rocks, which range from andesitic to dacitic to rhyolitic in composition (Sasso, 1997; Sasso and Clark, 1998).

The Capillitas diatreme represents one of the volcanic centers within the granitic basement block of the Sierra de Capillitas. It is composed of intrusive and volcaniclastic rocks (ignimbrite, rhyolite porphyry, dacite porphyry and tuffs) and is host to the epithermal vein-type Capillitas deposit, which is mainly known for the occurrence of gem-quality rhodochrosite. The epithermal veins are hosted in rhyolite, ignimbrite and granite and

show different types of host-rock alteration and both high sulfidation and intermediate sulfidation stage mineralization. The polymetallic character of the veins is reflected by its very complex mineralogy with the participation of Cu, Pb, Zn, Fe, As and Sb, associated with W, Bi, Sn, Te, Ag and Au as well as Ge, Cd, In, V, Ni and Tl. Further details on ore deposit geology, alteration and mineralization styles and ore mineralogy are presented elsewhere (e.g. Márquez-Zavalía, 1988, 1999; Paar *et al.*, 2004, Putz, 2005, Putz *et al.*, 2006, Putz *et al.*, 2009).

Cementation processes led to the formation of high-grade copper ores (bornite-chalcocite-digenite) which are restricted to the central part of the deposit in the vicinity of the La Rosario vein. As the old mine workings (“Mina La Rosario” and “Pique Rosario”) dating back to the 19th century are completely collapsed, material of this ore type is restricted to the old dumps nearby. Interestingly, only a few samples of this type of ore contain the unique assemblage of Ge minerals, such as putzite, catamarcaite, zincobriartite and omariniite (putzite-catamarcaite-omariniite-zincobriartite-paragenesis).

Intermediate-sulfidation stage veins hosted within the granitic basement (e.g. the La Argentina vein) are rich in galena, sphalerite and abundant rhodochrosite as the dominating gangue mineral. At the Santa Rita mine, where rhodochrosite-bearing ore of the La Argentina vein is currently mined for ornamental purposes, small-sized bonanza-grade ore bodies carry a silver-rich assemblage composed of proustite, pearceite, acanthite, native silver and argyrodite. The latter is locally intergrown with spryite, $\text{Ag}_8(\text{As}^{3+}_{0.5}\text{As}^{5+}_{0.5})\text{S}_6$ (Putz *et al.*, 2002; Putz, 2005; Bindi *et al.*, 2016).

The germanium-bearing minerals at Capillitas occur in two genetically different environments. The ore of the intermediate sulfidation stage was dictated by a high activity of silver and arsenic, which led to the formation of argyrodite-spryite. The increased

activity of copper within the ores created by supergene enrichment processes, however, led to the formation of copper-dominated phases, amongst them putzite. Further details dealing with the crystallization sequence of the omariniite-bearing ore and the possible conditions of formation are presented in Paar *et al.* (2004) and Putz *et al.* (2006).

APPEARANCE AND PHYSICAL PROPERTIES

Omariniite is fairly abundant in those bornite-chalcocite ores which also carry putzite and/or catamarcaite. Within the putzite holotype material, the new mineral frequently, but not exclusively, occurs as (1) a rim or seam at the contact between putzite and chalcocite, rarely exceeding a width of 60 μm but attaining a length of several hundreds of micrometers (Fig. 1a), and (2) as an envelope around the anhedral to subhedral inclusions of catamarcaite within putzite and chalcocite (Fig. 1b), where it is sometimes also associated with zincobriartite. The rims are usually composed of a mosaic of intensely twinned, anhedral subgrains (Figs. 1c and 1d); individual grains without twinning are rare and measure up to $30 \times 70 \mu\text{m}$. An exceptional single grain measures $200 \times 100 \mu\text{m}$. Wittichenite, tennantite, thalcusite and rare grains of mawsonite are also observed within this ore type but never in contact with omariniite.

The holotype material of catamarcaite also contains omariniite. Within this material, the new mineral occurs as (3) an envelope (generally below 10 μm in thickness) around catamarcaite inclusions within chalcocite/digenite/covellite/sphalerite in association with luzonite (see Fig. 3a in Putz *et al.*, 2006).

Omariniite is distinctly orange-brown, has a metallic luster, a reddish-brown streak and is opaque. It is brittle and has an irregular to sub-conchoidal fracture. Neither cleavage nor parting could be observed. Microhardness was determined with a Miniload 2 hardness

tester using loads of 25 and 100 g, respectively. While testing with a load of 100 g resulted in a VHN of 202 (range 190-215) kg.mm⁻², a distinctly higher VHN (534; 488-532 kg.mm⁻²) was obtained with a load of 25 g. The higher hardness at lower loads is related to elastic features of the tested material (Young and Millman, 1964). The calculated Mohs hardness using VHN₁₀₀ and the equation of Young and Millman (1964) is 3½.

The density could not be determined because of paucity of available material and the penetrative intergrowth with other phases. Using the unit-cell parameters from X-ray single crystal work and the ideal chemical formula, the calculated density is 4.319 g.cm⁻³. It is distinctly lower than the calculated density of stannoidite (4.68 g.cm⁻³; Kato, 1969).

OPTICAL PROPERTIES

In polished sections using plane-polarized light the color of omariniite is orange-brown which is enhanced in oil. Pleochroism is weak as also is the bireflectance. Between crossed polars, omariniite is distinctly anisotropic, with rotation tints changing from brownish-orange to greenish-brown. No internal reflections were observed.

Reflectance measurements were made using a J&M TIDAS diode array spectrometre between 400 and 700 nm at intervals of 0.8135 nm. The data were reduced to 20 nm intervals and are summarized in Table 1. A comparison of omariniite with stannoidite (Fig. 2) shows characteristic differences between the two species which allows them to be easily distinguished using optical methods. Both species show an increase of the reflectance values with increasing wavelength. The maxima for these minerals are towards the red end of the visible spectrum with dominant wavelengths (Λ_d) relative to the C illuminant of 590-597 nm (omariniite) and 577-578 nm (stannoidite) which explains the

orange-brown colors of the species in reflected light. However, the reflectance values for omariniite are generally markedly lower than those observed for stannoidite.

CHEMICAL COMPOSITION

Omariniite was analyzed with a JEOL Superprobe JXA-8600 (controlled by an LINK-eXL system, WDS mode, operated at 25kV and 35 nA, with 20s and 10s as counting times for peak and background, respectively), installed at the University of Salzburg, Austria. The following standards and X-ray lines were used: chalcopyrite (CuK α , FeK α), synthetic ZnS (ZnK α , SK α), Ge metal (GeK α), and synthetic InAs (InL α). Sn was sought but not detected. The raw data were processed with the on-line ZAF-4 program.

Several aggregates of omariniite in various polished sections of the putzite holotype material were analyzed and found to be homogeneous. The results show only minor variation of the chemical composition (Table 2). The average result of 45 point analyses of three grain aggregates is (wt.%): Cu 42.18(34), Fe 9.37(26), Zn 5.17(43), In 0.20(6), Ge 11.62(22), S 31.80(20), total 100.34(46). Using the ideal formula of stannoidite, Cu₈Fe₂ZnSn₂S₁₂, and $\sum Me + S = 25$, this corresponds to Cu_{8.04}(Fe_{2.03}In_{0.02})_{Σ2.05}Zn_{0.96}Ge_{1.94}S_{12.01}. The ideal chemical formula of omariniite, with valence states for the elements in agreement with those reported for stannoidite by Yamanaka and Kato (1976), can be expressed as Cu⁺₈Fe³⁺₂Zn²⁺Ge⁴⁺₂S²⁻₁₂ which requires Cu 41.83, Fe 9.19, Zn 5.38, Ge 11.95, S 31.65, total 100.00 wt.%

X-RAY CRYSTALLOGRAPHY AND CRYSTAL-STRUCTURE DETERMINATION

Few omariniite crystals were handpicked from a polished section under a reflected light microscope and examined by means of an Oxford Diffraction Xcalibur 3 CCD single-

crystal diffractometer using graphite-monochromatized MoK α radiation (see Table 3 for details). Single-crystal X-ray diffraction intensity data were integrated and corrected for standard Lorentz-polarization factors with the *CrysAlis* RED package (Oxford Diffraction, 2006). The program ABSPACK in *CrysAlis* RED (Oxford Diffraction, 2006) was used for the absorption correction. A total of 1238 unique reflections was collected. The statistical tests on the distribution of $|E|$ values ($|E^2 - 1| = 0.697$) indicated the absence of an inversion center. Systematic absences were consistent with the space group *I*222.

Given the similarity in the unit-cell values and in the space groups, the structure was refined starting from the atomic coordinates reported for stannoidite (Kudoh and Takéuchi, 1976) using the program Shelxl-97 (Sheldrick, 2008). The site occupation factor (s.o.f.) at the seven cation sites was allowed to vary (Zn vs. structural vacancy) using scattering curves for neutral atoms taken from the *International Tables for Crystallography* (Wilson, 1992). After several cycles and a careful check of the bond distances at the different sites, the positions were found fully occupied by the atomic species given in Table 4 and their s.o.f. were fixed to 1. Only at the M5 site the electron density was found higher than 26 (pure occupation by Fe) and all the In³⁺ found by electron microprobe was thought to occur at this site. Table 3 reports details of the selected crystal, data collection, and refinement. Final atomic coordinates and equivalent isotropic displacement parameters are given in Table 4, whereas selected bond distances are shown in Table 5. A list of the observed and calculated structure factors and CIF are deposited with the Principal Editor of Mineralogical Magazine at http://www.minersoc.org/pages/e_journals/dep_mat.html.

DESCRIPTION OF THE STRUCTURE AND RELATIONSHIPS WITH OTHER SPECIES

The crystal structure of omariniite (Fig. 3) can be considered as a sphalerite derivative. The omariniite structural topology is also derivable from the stannite structure by substituting Cu atoms for a set of Ge atoms in stannite and adding excess Cu atoms in a set of tetrahedral vacancies (Fig. 4). A comparison of the bond distances for the different tetrahedra occurring in stannoidite and omariniite is presented in Table 5. It appears evident that the Ge-tetrahedron (*i.e.* M6) is much smaller (mean bond distance 2.248 Å) than the Sn-homologue in stannoidite (mean bond distance 2.40 Å; Kudoh and Takéuchi, 1976) and it is close to that observed in argyrodite (2.212 Å; Eulenberger, 1977) and in putzite (2.192 Å; Paar *et al.*, 2004). The Zn-tetrahedron (*i.e.* M1) is larger (2.447 Å) than the equivalent site in stannoidite (2.35 Å; Kudoh and Takéuchi, 1976), which exhibits a $\text{Zn}_{0.85}\text{Fe}_{0.15}$ site population. Likewise, the Fe-tetrahedron (*i.e.* M5) is larger (2.379 Å) than the equivalent site in stannoidite (2.34 Å; Kudoh and Takéuchi, 1976), due to the presence of the minor amounts of In^{3+} replacing Fe^{3+} .

Due to the iso-electronic nature of its constituent elements (Fe = 26, Cu = 29, Zn = 30, Ge = 32) together with the ambiguity in their valence states, the metal partitioning in omariniite is, however, not straightforward. According to Brese and O'Keeffe (1991), the ideal *Me*–S distance (in Å) in a regular tetrahedron decreases following the sequence: 2.466/ In^{3+} , 2.450/ Sn^{4+} , 2.416/ Fe^{2+} , 2.370/ Cu^{+} , 2.346/ Zn^{2+} , 2.266/ Fe^{3+} , 2.220/ Ge^{4+} , 2.116/ Cu^{2+} . Consequently, Ge^{4+} should be hosted within the smallest tetrahedron (*i.e.* M6), whereas Fe^{3+} should be hosted at the other small tetrahedral sites. Taking into account this approach for both stannoidite and omariniite structures, a bond valence balance give the following values for the M sites (values for stannoidite and omariniite, respectively, are given in parentheses in valence units, v.u.): M1 (2.04, 1.52), M2 (1.36, 1.36), M3 (1.22,

1.23), M4 (1.13, 0.86), M5 (2.48, 2.26), M6 (4.59, 3.72), M7 (1.19, 1.28). Recent studies demonstrated the presence of Cu^+ and Fe^{3+} in chalcopyrite (e.g., Goh *et al.*, 2006) and the corresponding bond-valence sums (BVS) at Cu and Fe sites are 1.18 and 3.15 v.u., respectively, with corresponding bond distances of 2.312 and 2.248 Å (Knight *et al.*, 2011). Consequently, the bond valence sums at Cu sites (M2, M3, M4, M7) in both the stannoidite and omariniite structures probably agree with the presence of Cu^+ . Such an oversaturation at Cu tetrahedral sites have been observed in other sulfides and sulfosalts and it could probably be related to the non-accuracy of the bond parameter for Cu–S bond given by Brese and O'Keeffe (1991) and to the covalent nature of the bonds. On the contrary, the observed strong undersaturation at M1 (in omariniite) and M5 (both stannoidite and omariniite) have to be taken into account. They could be either related to some limits in the crystal structure refinement or to a different metal partitioning. A possible hypothetical new partition could be Cu^+ at M1 (BVS 0.82), Fe^{3+} at M2 (BVS 3.07), Fe^{3+} at M3 (BVS 2.76), Cu^+ at M4 (BVS 0.86), $(\text{Cu}^{+}_{0.5}\text{Zn}^{2+}_{0.5})$ at M5 (BVS 1.41), Ge^{4+} at M6 (BVS 3.72), and Cu^+ at M7 (BVS 1.28), giving rise to the formula $\text{Cu}^+_8\text{Fe}^{3+}_2\text{ZnGe}^{4+}_2\text{S}_{12}$ ($Z = 2$).

Calculated X-ray powder diffraction data (d in Å) for omariniite are given in Table 6. Intensities and d_{hkl} values were calculated using the Powdercell 2.3 software (Kraus and Nolze, 1996) on the basis of the structural model given in Table 4.

There probably exists a solid solution series between stannoidite and omariniite, as stannoidite from Tsumeb and Khusib Springs carry significant germanium (0.5–0.7 wt.% in Khusib Springs and up to 2.2 wt.% in Tsumeb, respectively; Melcher, 2003).

ACKNOWLEDGEMENTS

Thanks are due to Dan Topa, Peter Leverett and one anonymous reviewer for their insightful comments. This work has been partially funded by “Progetto d’Ateneo 2014” from the University of Firenze to LB. WHP expresses his thanks to the Austrian Science Foundation (FWF) which supported through grant #13974 field work in Argentina. We thank Prof. Ricardo Sureda for logistical help during several visits at Capillitas. We are grateful to Mark A. Cooper and Andrew C. Roberts for the first investigations of the new mineral. Last but not least, HP say thanks to the Yampa family at Andalgalá, owner of the Santa Rita mine at Capillitas, who provided great hospitality of Argentinian style during numerous stays at Capillitas.

REFERENCES

- Bindi, L., Keutsch, F.N. and Zaccarini, F. (2016) Spryite, IMA 2015-116. CNMNC Newsletter No. 30, April 2016, page 412. *Mineralogical Magazine*, **80**, 407–413.
- Brese, N.E. and O’Keeffe, M. (1991) Bond-valence parameters for solids. *Acta Crystallographica*, **B47**, 192-197.
- Effenberger, H., Lengauer, C.L., Libowitzky, E., Putz, H. and Topa, D. (2015) Lislkirchnerite, IMA 2015-064. CNMNC Newsletter No. 27, October 2015, page 1230. *Mineralogical Magazine*, **79**, 1229–1236.
- Eulenberger, G. (1977) Die Kristallstruktur der Tieftemperaturmodifikation von Ag_8GeS_6 . *Monatshefte für Chemie*, **108**, 901–913.
- Goh, S.W., Buckley, A.N., Lamb, R.N., Rosenberg, R.A. and Moran, D. (2006) The oxidation states of copper and iron in mineral sulfides, and the oxides formed on

initial exposure of chalcopyrite and bornite to air. *Geochimica et Cosmochimica Acta*,
70, 2210-2228.

Höll, R., Kling, M. and Schroll, E. (2007) Metallogenesis of germanium - a review. *Ore
Geology Reviews*, **30**, 145–180.

Kato, A. (1969) Stannoidite, $\text{Cu}_5(\text{Fe,Zn})_2\text{SnS}_8$, a new stannite-like mineral from the Konjo
mine, Okayama Prefecture, Japan. *Bulletin of the National Science Museum Tokyo*,
12, 165–172.

Knight, K.S., Marshall, W.G. and Zochowski, S.W. (2011) The low temperature and high-
pressure thermoelastic and structural properties of chalcopyrite, CuFeS_2 . *Canadian
Mineralogist*, **49**, 1015-1034.

Kraus, W. and Nolze, G. (1996) PowderCell – a program for the representation and
manipulation of crystal structures and calculation of the resulting X-ray powder
patterns. *Journal of Applied Crystallography*, **29**, 301–303.

Kudoh, Y. and Takéuchi, Y. (1976) The superstructure of stannoidite. *Zeitschrift für
Kristallographie*, **144**, 145–160.

Márquez-Zavalía, M.F. (1988) *Mineralogía y genesis del yacimiento Capillitas (Catamarca,
Republica Argentina)*. Ph.D.thesis, University of Salta, Salta, Argentina.

Márquez-Zavalía, M.F. (1999) El yacimiento Capillitas, Catamarca. In Recursos minerales
de la República Argentina (O. Zappettini, ed.). *Instituto de Geología y Recursos
Minerales SEGEMAR, Anales* **35**, 1643–1652.

Márquez-Zavalía, M.F., Galliski, M.A., Drábek, M., Vymazalová, A., Watanabe, Y.,
Murakami, H. and Bernhardt, H.-J. (2015) Ishiharaite, $(\text{Cu,Ga,Fe,In,Zn})\text{S}$, a new
mineral from the Capillitas mine, Northwestern Argentina. *Canadian Mineralogist*, **52**,
969–980.

320 McDonald, A.M., Stanley, C.J., Ross, K.C. and Nestola, F. (2016) Zincobriartite, IMA 2015-
 321 094. CNMNC Newsletter No. 29, February 2016, page 203. *Mineralogical Magazine*,
 322 **80**, 199-205.

323 Melcher, F. (2003) The Otavi Mountain Land in Namibia: Tsumeb, germanium and
 324 snowball earth. *Mitteilungen der Österreichischen Mineralogischen Gesellschaft*, **148**,
 325 413–435.

326 Oxford Diffraction (2006) *CrysAlis* RED (Version 1.171.31.2) and ABSPACK in *CrysAlis*
 327 RED. Oxford Diffraction Ltd, Abingdon, Oxfordshire, England.

328 Paar, W.H. and Putz, H. (2005) Germanium associated with epithermal mineralization:
 329 examples from Bolivia and Argentina. *8th Biennial SGA Meeting (Beijing)*,
 330 Proceedings 3, 48–51.

331 Paar, W.H., Roberts, A.C., Berlepsch, P., Armbruster, T., Topa, D. and Zagler, G. (2004)
 332 Putzite, $(\text{Cu}_{4.7}\text{Ag}_{3.3})_{\Sigma 8}\text{GeS}_6$, a new mineral species from Capillitas, Catamarca,
 333 Argentina: description and crystal structure. *Canadian Mineralogist*, **42**, 1757–1769.

334 Putz, H. (2005) *Mineralogy and Genesis of Epithermal Ore Deposits at Capillitas,*
 335 *Catamarca Province, NW-Argentina*. Ph.D. thesis, Salzburg Univ., Salzburg, Austria.

336 Putz, H., Paar, W.H., Sureda, R.J. and Roberts, A.C. (2002) Germanium mineralization at
 337 Capillitas, Catamarca Province, Argentina. *IMA 18th Gen. Meeting (Edinburg)*,
 338 Abstracts, 265.

339 Putz, H., Paar, W.H., Topa, D., Makovicky, E. and Roberts, A.C. (2006) Catamarcaite,
 340 Cu_6GeWS_8 , a new germanium sulfide mineral species from Capillitas, Catamarca,
 341 Argentina: Description, Paragenesis and Crystal Structure. *Canadian Mineralogist*,
 342 **44**, 1481–1497.

- Putz, H., Paar, W.H. and Topa, D. (2009) A contribution to the knowledge of the mineralization at Capillitas, Catamarca. *Revista de la Asociación Argentina*, **64**(3), 514–524.
- Sasso A.M. (1997) *Geological Evolution and Metallogenetic Relationships of the Farallón Negro Volcanic Complex, NW Argentina*. Ph.D.thesis, Queen's Univ., Kingston, Ontario.
- Sasso, A.M. and Clark, A.H. (1998) The Farallon Negro group, northwest Argentina: magmatic, hydrothermal and tectonic evolution and implications for Cu-Au metallogeny in the Andean back-arc. *Society of Economic Geology, Newsletter*, **34**, 1–18.
- Sheldrick, G.M. (2008) A short history of SHELX. *Acta Crystallographica*, **A64**, 112–122.
- Yamanaka, T. and Kato, A. (1976) Mössbauer effect study of ⁵⁷Fe and ¹¹⁹Sn in stannite, stannoidite, and mawsonite. *American Mineralogist*, **61**, 260-265.
- Young, B.B. and Millman, A.P. (1964) Microhardness and deformation characteristics of ore minerals. *Transactions of the Institution of Mining and Metallurgy*, **73**, 437-466.
- Wilson, A.J.C., Ed. (1992) *International Tables for Crystallography*, Volume C: Mathematical, physical and chemical tables. Kluwer Academic, Dordrecht, NL.

FIGURE CAPTIONS

Figure 1: Different associations of omariniite. (a) Putzite (pu) rimmed by omariniite (om) in association with chalcocite (cc) containing relics of bornite (bo); late-stage sphalerite (sp) in narrow veinlets is crosscutting chalcocite and the Ge sulfides (sample PR/C2). Air, uncrossed polars. (b) Omariniite (om) is seaming catamarcaite (cat) which locally shows sub- to euhedral crystal forms. These composite grains represent inclusions within putzite (pu) which is strongly replaced by chalcocite (cc) and late-stage sphalerite (sp); zincobriartite (zbt) occurs in traces (sample PR/C3P). Air, uncrossed polars. (c) Rim of omariniite (om; with weak pleochroism) in association with putzite (pu), catamarcaite (cat), chalcocite (cc), bornite (bn) and sphalerite (sp); (sample PR/C2). Air, uncrossed polars. (d) Same field of view as in panel (c) omariniite (om) shows its characteristic anisotropy with orange-brown to greenish grey rotation-tints (sample PR/C2). Air, crossed polars.

Figure 2: Reflectance spectra, in air, for omariniite and stannoidite.

Figure 3: Crystal structure of omariniite. Filled circles: black = Zn; light blue = Cu; orange = Fe; dark blue: Ge; yellow = S.

Figure 4: Atoms distribution seen down [010] showing the cation ordering leading to the occurrence of the superstructure of the stannite structure. The unit cell of stannite is indicated with dashed lines. Symbols as in Figure 6.

TABLES

Table 1: Reflectance data for omariniite

Table 2: Composition of omariniite.

Table 3: Crystal and experimental data for omariniite.

Table 4: Wyckoff positions, site occupation factors, fractional atomic coordinates, and equivalent isotropic displacement parameters (\AA^2) for the selected omariniite crystal.

Table 5: Comparison of the bond distances (\AA) in the crystal structure of stannoidite (1; Kudoh & Takéuchi 1976) and omariniite (2; this study).

Table 6: Calculated X-ray powder diffraction data (d in \AA) for omariniite. Intensities and d_{hkl} values were calculated using Powdercell 2.3 software (Kraus & Nolze 1996) on the basis of the structural model given in Table 4; only reflections with $I_{\text{calc}} > 1$ are listed. Strongest reflections are given in bold.

Table 1. Reflectance data and color values for omariniite

λ (nm)		omariniite		stannoidite	
		R1	R2	R1	R2
400		22.0	21.9	17.5	18.9
420		20.9	21.5	17.4	19.2
440		20.2	21.0	18.2	20.3
460		19.7	21.0	19.5	21.7
480		19.5	21.0	20.8	23.0
500		19.4	21.1	21.8	24.2
520		19.75	21.4	22.8	25.3
540		20.4	21.8	23.7	26.3
560		21.2	22.2	24.6	27.1
580		22.1	22.8	25.4	27.8
600		23.2	23.5	26.2	28.4
620		24.2	24.2	27.1	29.1
640		25.3	25.0	27.85	29.5
660		26.2	25.7	28.7	30.0
680		27.2	26.6	29.6	30.5
700		28.2	27.4	30.3	30.8

C illumin	x	0.328	0.322	0.339	0.335
	y	0.320	0.321	0.343	0.342
	Y%	21.4	22.4	24.4	26.8
	Lambda				
	d	597	590	578	577
	Pe%	5.9	4.7	14.8	13.8
A	x	0.467	0.461	0.471	0.468
	y	0.403	0.406	0.414	0.415
	Y%	22.0	22.8	25.1	27.4
	Lambda				
	d	616	616	587	586
	Pe%	8.0	5.3	20.8	18.9

Table 2. Electron microprobe analyses (means, standard deviations and ranges in wt. % of elements) for omariniite.

Cu	42.18(34)	41.46-43.13
Fe	9.37(26)	8.94-10.20
Zn	5.17(43)	4.30-5.96
In	0.20(6)	0.10-0.30
Ge	11.62(22)	11.04-12.02
S	31.80(20)	31.41-32.30
Total	100.34(46)	99.33-101.13

Table 3. Crystal and experimental data for omariniite.

<i>Crystal data</i>	
Crystal size (mm ³)	0.05 × 0.06 × 0.07
Cell setting, space group	Orthorhombic, <i>I</i> 222
<i>a</i> (Å)	10.774(1)
<i>b</i> (Å)	5.3921(5)
<i>c</i> (Å)	16.085(2)
<i>V</i> (Å ³)	934.5(2)
<i>Z</i>	2
<i>Data collection and refinement</i>	
Radiation, wavelength (Å)	MoKα, λ = 0.71073
Temperature (K)	293
2θ _{max} (°)	59.97
Measured reflections	10125
Unique reflections	1238
Reflections with <i>F</i> _o > 4σ(<i>F</i> _o)	432
<i>R</i> _{int}	0.0423
<i>R</i> σ	0.0268
Range of <i>h</i> , <i>k</i> , <i>l</i>	−13 ≤ <i>h</i> ≤ 13, −7 ≤ <i>k</i> ≤ 7, −22 ≤ <i>l</i> ≤ 22
<i>R</i> [<i>F</i> _o > 4σ(<i>F</i> _o)]	0.0226
<i>R</i> (all data)	0.0273
<i>wR</i> (on <i>F</i> ²)	0.0462
GooF	0.990
Number of least-squares parameters	62
Max. and min. resid. peak (e Å ^{−3})	0.43 (at 0.29 Å from S2) −1.82 (at 0.96 Å from M6)

Table 4. Wyckoff positions, site occupation factors, fractional atomic coordinates, and equivalent isotropic displacement parameters (\AA^2) for the selected omariniite crystal.

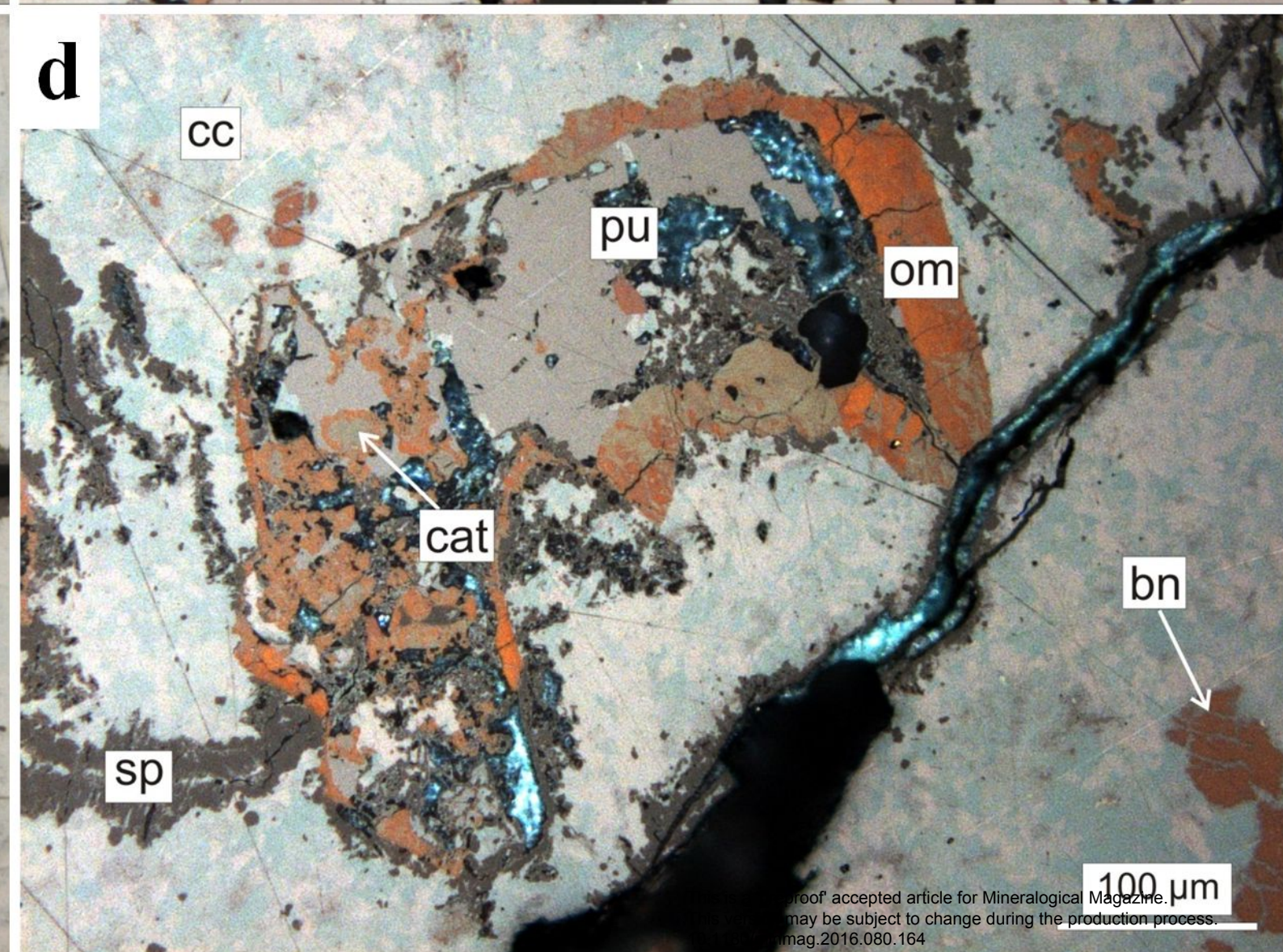
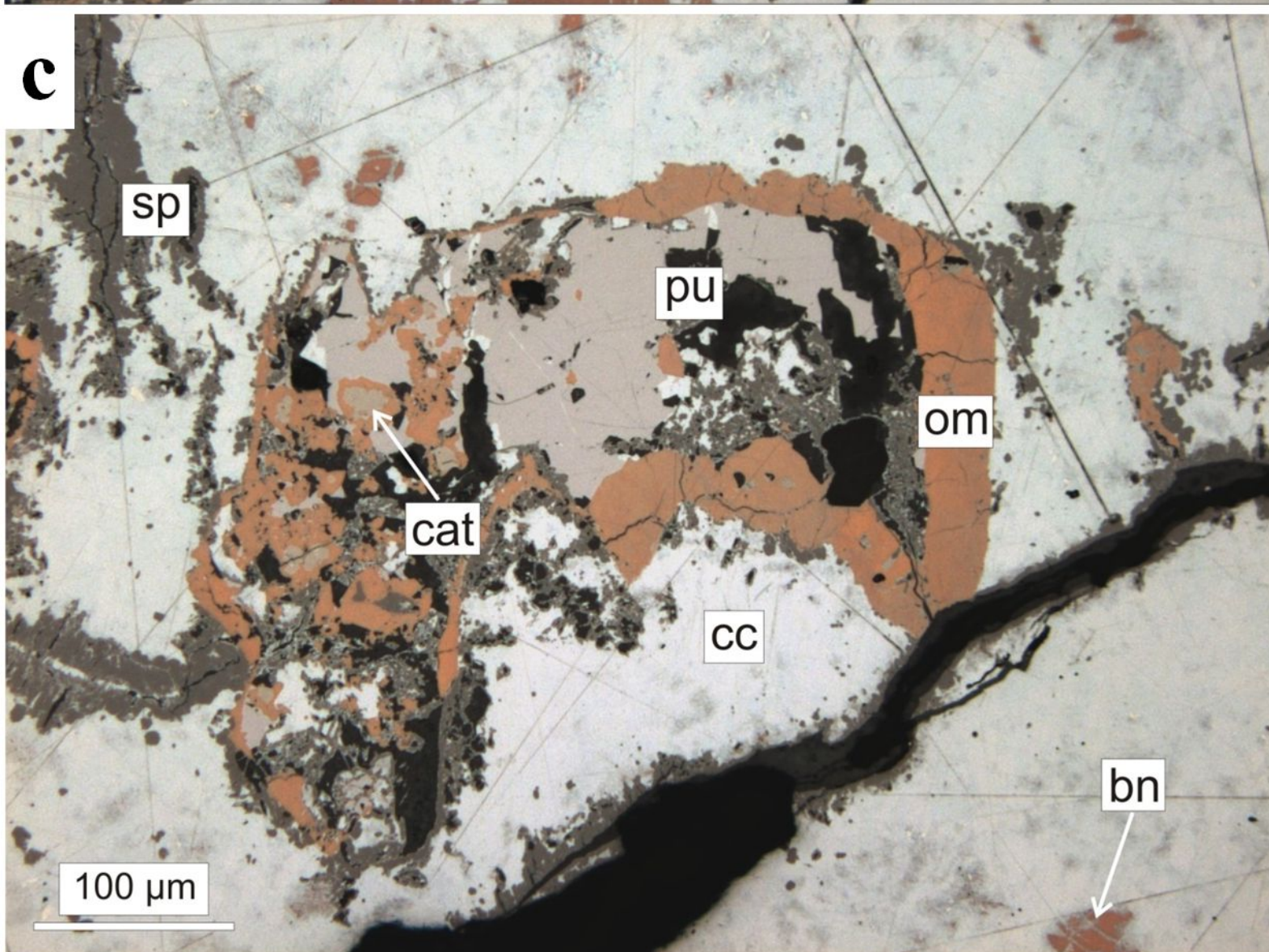
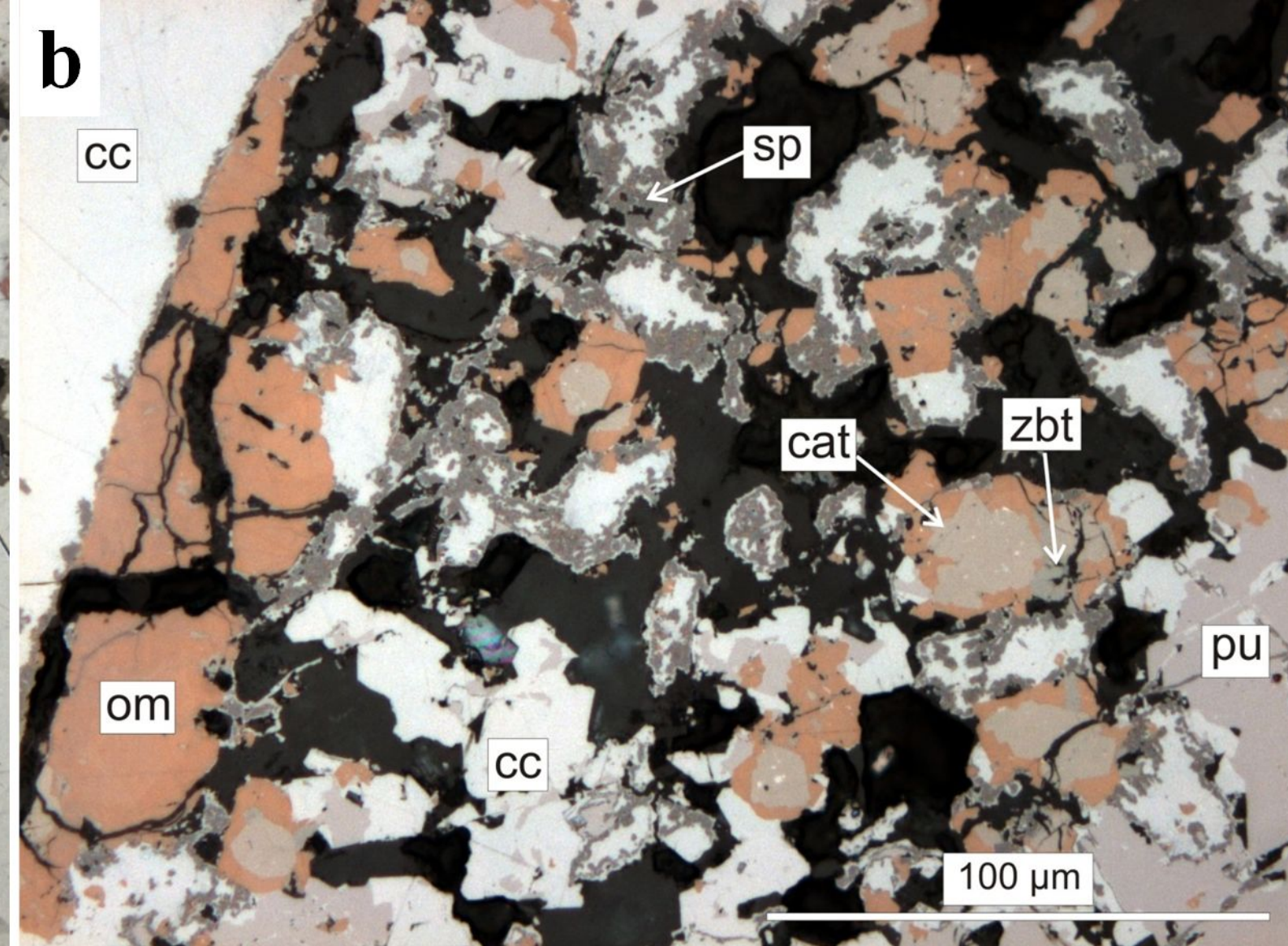
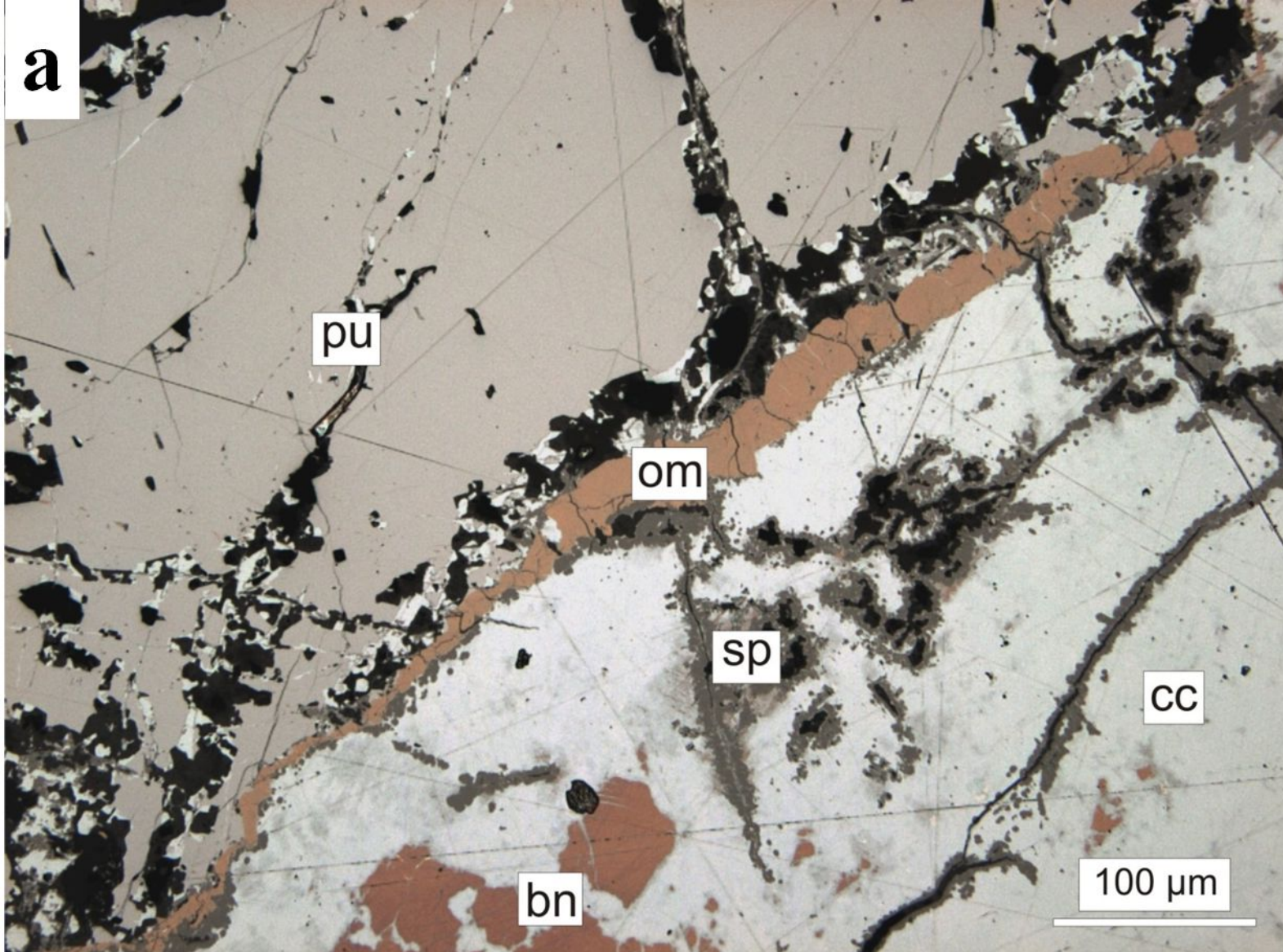
atom	Wyckoff	s.o.f.	x	y	z	U_{iso}
M1	2a	Zn _{1.00}	0	0	0	0.0238(4)
M2	2b	Cu _{1.00}	½	0	0	0.0208(4)
M3	2c	Cu _{1.00}	0	0	½	0.0238(4)
M4	4f	Cu _{1.00}	0.25821(14)	0	½	0.0196(3)
M5	4i	Fe _{0.97(1)} In _{0.03}	0	0	0.32997(11)	0.0242(5)
M6	4j	Ge _{1.00}	0	½	0.17651(9)	0.0234(3)
M7	8k	Cu _{1.00}	0.24616(11)	0.0105(2)	0.16974(6)	0.0245(2)
S1	8k	S _{1.00}	0.1218(3)	0.2463(7)	0.09836(18)	0.0368(7)
S2	8k	S _{1.00}	0.3797(4)	0.7553(8)	0.08051(18)	0.0413(9)
S3	8k	S _{1.00}	0.1293(3)	0.7482(8)	0.2446(3)	0.0415(7)

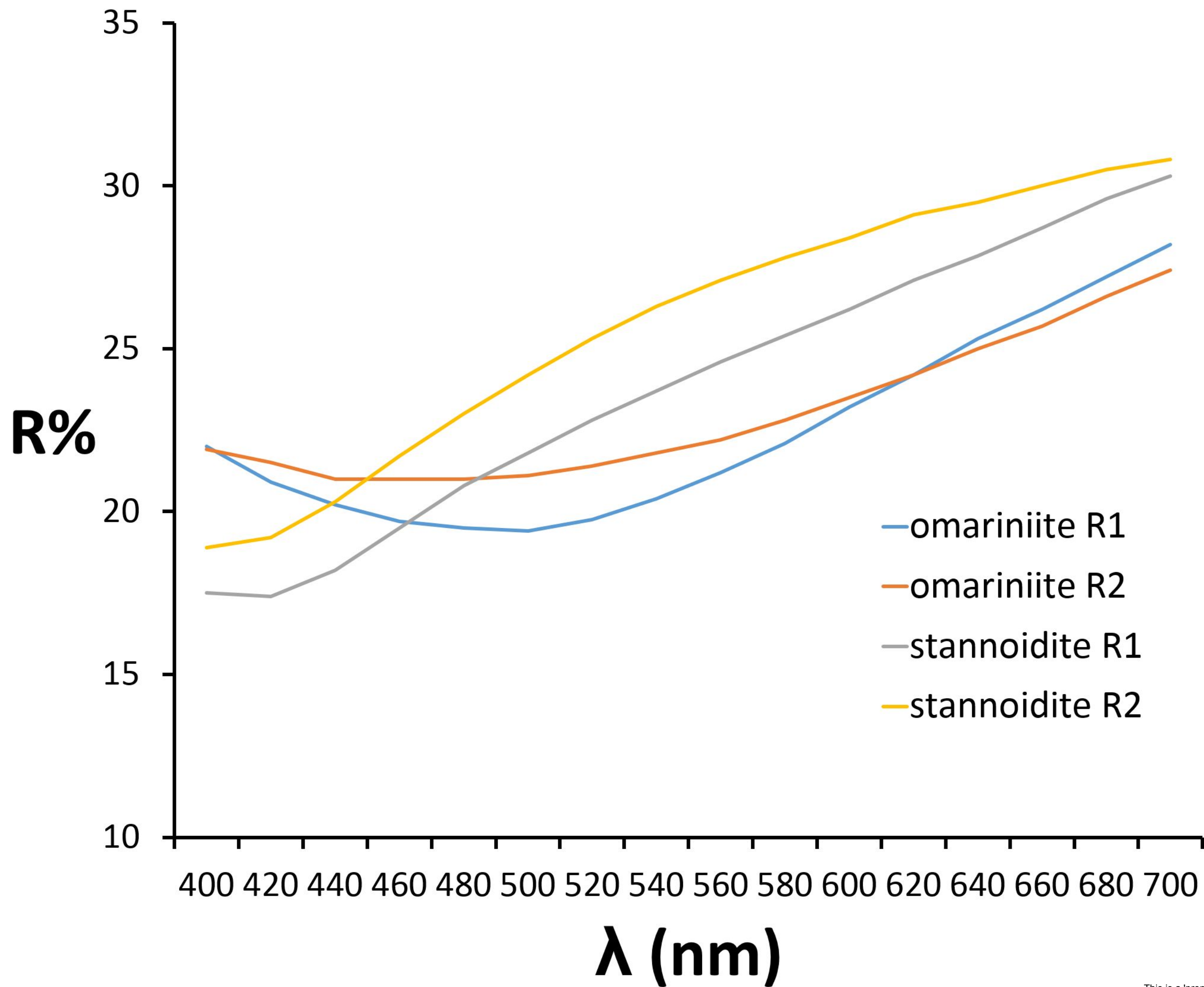
Table 5. Comparison of the bond distances (Å) in the crystal structure of stannoidite (1; Kudoh and Takéuchi, 1976) and omariniite (2; this study).

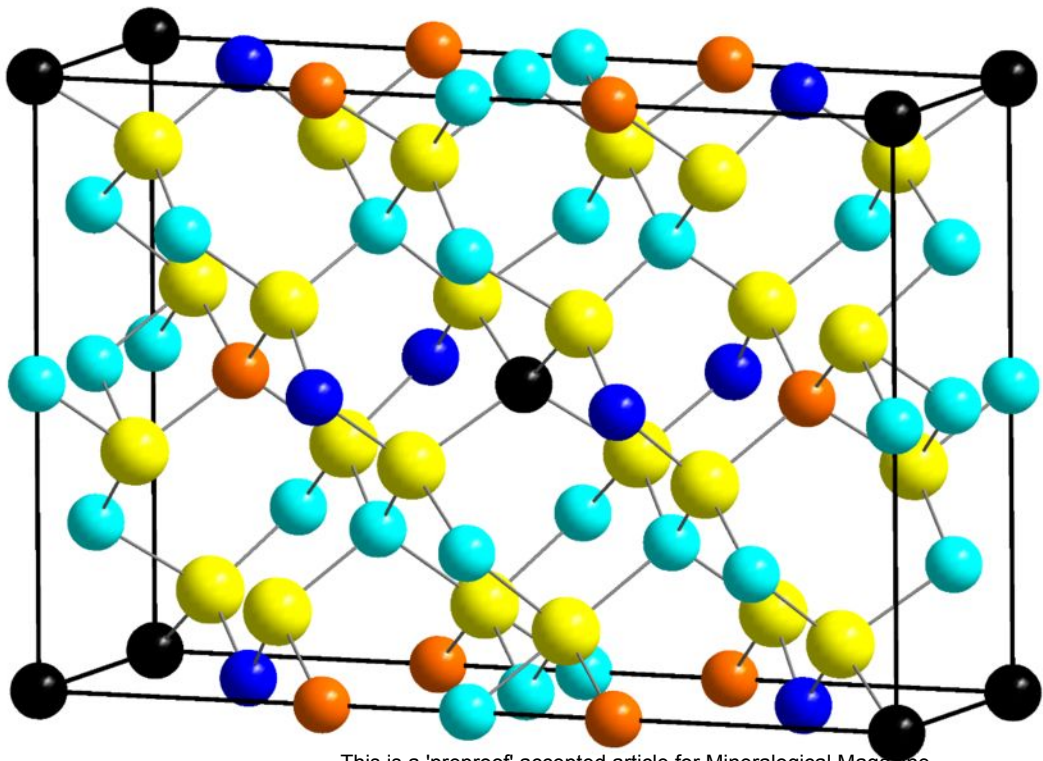
	1	2
M1-S1 (×4)	2.346	2.447(3)
M2-S2 (×4)	2.259	2.258(4)
M3-S2 (×4)	2.297	2.292(4)
M4-S1 (×2)	2.303	2.459(4)
M4-S2 (×2)	2.356	2.404(4)
M5-S2 (×2)	2.391	2.377(4)
M5-S3 (×2)	2.293	2.381(4)
M6-S1 (×2)	2.419	2.275(4)
M6-S3 (×2)	2.376	2.220(3)
M7-S1	2.261	2.175(4)
M7-S2	2.454	2.454(4)
M7-S3	2.341	2.244(4)
M7-S3	2.223	2.311(4)

Table 6. Calculated X-ray powder diffraction data (d in Å) for omariniite. Intensities and d_{hkl} values were calculated using Powdercell 2.3 software (Kraus and Nolze, 1996) on the basis of the structural model given in Table 5; only reflections with $I_{\text{calc}} > 1$ are listed. Strongest reflections are given in bold.

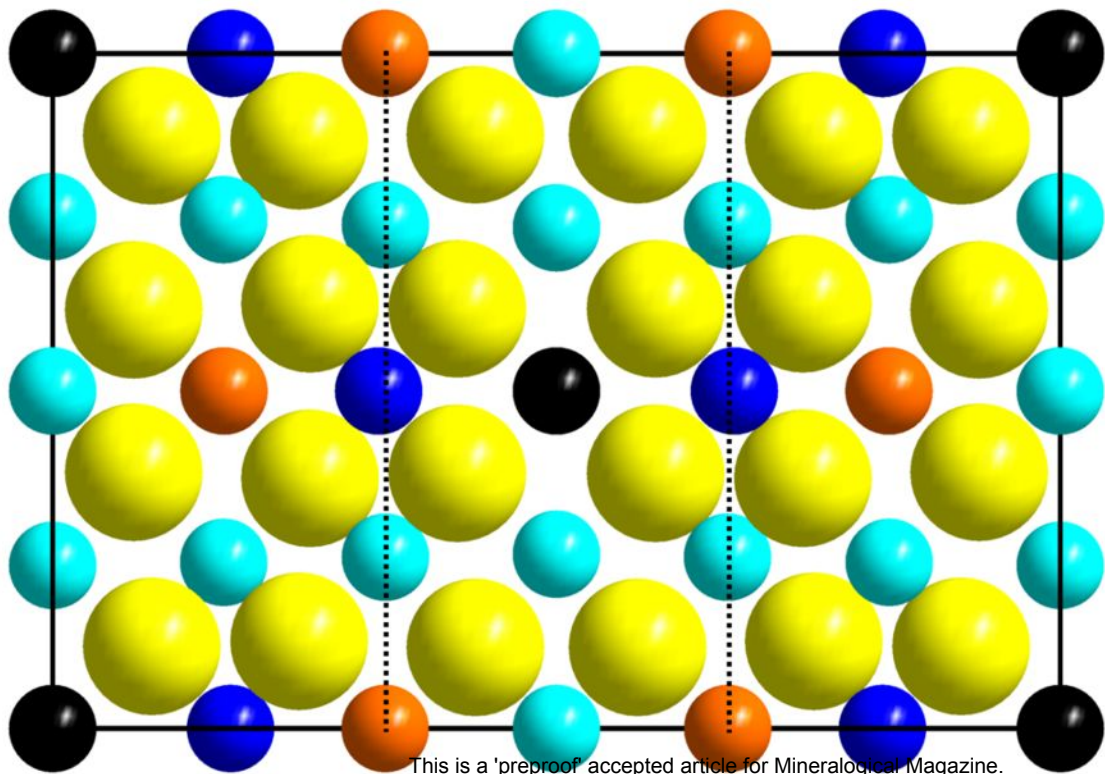
I_{rel}	d_{calc} (Å)	hkl
2	8.9515	101
4	4.8001	103
1	4.4757	202
2	4.1356	112
100	3.1063	213
2	2.8018	312
6	2.6960	020
6	2.6935	400
6	2.6808	006
1	2.4583	215
24	1.9055	420
23	1.9010	026
23	1.9001	406
12	1.6248	233
12	1.6237	613
11	1.6181	219
4	1.5531	426
3	1.3480	040
3	1.3468	800
3	1.3404	0012
4	1.2361	633
4	1.2336	239
4	1.2332	619
6	1.0994	446
6	1.0989	826
5	1.0963	4212
2	1.0375	253
2	1.0366	1013
2	1.0354	639
2	1.0322	2115







This is a 'preproof' accepted article for Mineralogical Magazine.
This version may be subject to change during the production process.
10.1180/minmag.2016.080.164



This is a 'preproof' accepted article for Mineralogical Magazine.
This version may be subject to change during the production process.
10.1180/minmag.2016.080.164